Combustion and Flame 158 (2011) 2037–2044

Contents lists available at ScienceDirect

Combustion and Flame

journal homepage: www.elsevier.com/locate/combustflame

Unified behaviour of maximum soot yields of methane, ethane and propane laminar diffusion flames at high pressures

Ömer L. Gülder *, Gorngrit Intasopa, Hyun I. Joo, Paul M. Mandatori, Décio S. Bento, Marie E. Vaillancourt

University of Toronto, Institute for Aerospace Studies, 4925 Dufferin Street, Toronto, Ontario, Canada M3H 5T6

ARTICLE INFO

Article history:
Received 19 November 2010
Received in revised form 21 March 2011
Accepted 24 March 2011
Available online 18 April 2011

Keywords:
High-pressure combustion
High-pressure soot formation
Supercritical combustion
Unified soot yield at high pressures

ABSTRACT

Soot concentration and temperature distributions within the flame envelope of laminar diffusion flames of methane and ethane at elevated pressures were measured in a high-pressure combustion chamber. Methane measurements were made with two different fuel flow rates: 0.43 mg/s (0.32 mg/s carbon flow rate) for the pressure range of 15–60 atm, and 0.83 mg/s for the pressure range of 5–20 atm (0.62 mg/s carbon flow rate). For the ethane flames, the flow rate was 0.78 mg/s (0.62 mg/s carbon flow rate) and the pressure range was 2–15 atm. From the soot concentration distribution, soot yields were calculated as a function of flame height and pressure. Maximum soot yields from the current study and the previous measurements in similar flames with methane, ethane, and propane flames were shown to display a unified behaviour. Maximum soot yields, when scaled properly, were represented by an empirical exponential function in terms of the reduced pressure, actual pressure divided by the critical pressure of the fuel. The maximum soot yield seems to reach a plateau asymptotically as the pressure exceeds the critical pressure of the fuel.

1. Introduction

For optimal efficiency and size, combustion process in propulsion devices and engines is turbulent and is designed to take place at elevated pressures because the combustion intensity, that is energy released per unit volume, scales roughly with the square of pressure. However the pressure has a significant effect on the overall soot yield as well as on the rates of soot production and oxidation in diffusion flames. But the experimental study of soot formation processes in turbulent diffusion flames at elevated pressures is not trivial. Reliable measurements of spatially and temporally resolved soot concentrations and oxidation rates in unsteady turbulent flames with shorter residence times are not usually tractable [1], especially at elevated pressures, whereas such measurements are relatively easy in laminar diffusion flames. As a consequence, most of the soot measurements are made in laminar diffusion flames that provide easily controlled conditions and the results can be projected to practical turbulent flames using the approximate approaches like the flamelet hypothesis. The flamelet hypothesis assumes that turbulent flames are collections of distorted laminar flames with reaction zone structures similar to laminar flames.

Experimental research in laminar diffusion flames under elevated pressures have been held back by the complications in designing an experimental apparatus and in operating instruments that require accessibility for intrusive and non-intrusive measurement techniques [1]. In addition, the stability of laminar diffusion flames, especially originating from buoyancy effects, becomes an important issue at elevated pressures due to the increase in Grashoff number which scales with the square of pressure. These impediments have limited the number and the extent of experimental soot studies in laminar diffusion flames at elevated pressures.

As pressure is increased, measured soot volume fractions increase since the flame narrows and the soot flows through a smaller cross-section. This narrowing of the flame causes local temperature gradients near the centerline to increase and fuel pyrolysis rates in the central core to intensify. Enhanced air entrainment into the flame near the burner is also expected to increase pyrolysis rates [2]. Miller and Maahs [3] estimated total soot concentrations in high-pressure axisymmetric methane–air diffusion flames between 1 and 50 atm from measurements of the flame emissive power. The data indicate that soot yield is proportional to P^n, where n is approximately 1.7–0.7 up to 10 atm. Above 10 atm, the dependence of soot yield on pressure decreased significantly.

Flower and Bowman [4] studied laminar diffusion flames of ethylene at pressures between 1 and 10 atm by measuring line-of-sight integrated soot volume fractions and temperatures along the flame centerline. They reported maximum diameter-integrated soot volume fractions proportional to $P^{1.2}$. Measurements made by

* Corresponding author. Fax: +1 416 667 7799.
E-mail address: ogulder@utias.utoronto.ca (Ö.L. Gülder).

0010-2180/$ - see front matter © 2011 The Combustion Institute. Published by Elsevier Inc. All rights reserved.
doi:10.1016/j.combustflame.2011.03.010

Lee et al. [5] in laminar ethylene diffusion flames from 1 to 4 atm indicated a $P^{1.26}$ dependence of the maximum diameter-integrated soot volume fraction on pressure. McCrain and Roberts [6] obtained similar pressure exponents in methane flames from 1 to 25 atm and ethylene flames from 1 to 16 atm based on path-integrated and local soot volume fraction measurements. Radially-resolved soot concentration and temperature measurements were reported by Thomson et al. [7] for methane diffusion flames from 5 to 40 atm. These measurements were later extended to 60 atm by Joo and Gülder [8]. Both concluded that the maximum amount of fuel carbon converted to soot, which is most suitable for assessing the sensitivity of soot formation to pressure [4], varied proportional to pressure between 5 and 20 atm. Between 30 and 60 atm, Joo and Gülder measured a pressure exponent equal to 0.33. Similar soot and temperature measurements were made by Bento et al. [9] for propane flames from 1 to 7.2 atm, and by Mandatori and Gülder [10] for ethane flames from 2 to 33 atm.

The first objective of the research reported in this paper was to determine soot yields in co-flow methane–air and ethane–air laminar diffusion flames at elevated pressures at different fuel flow rates than reported previously. The soot yield is defined as the mass flow of soot at a given flame height cross-section per mass flow of carbon in the fuel. The second objective was to investigate whether the pressure dependence of soot yield in various gaseous diffusion flames is similar. Available high-pressure soot yield data from our previous gaseous diffusion flames, when combined with the new data sets obtained in this work, were shown to display a unified dependence on pressure when the soot yield is properly scaled.

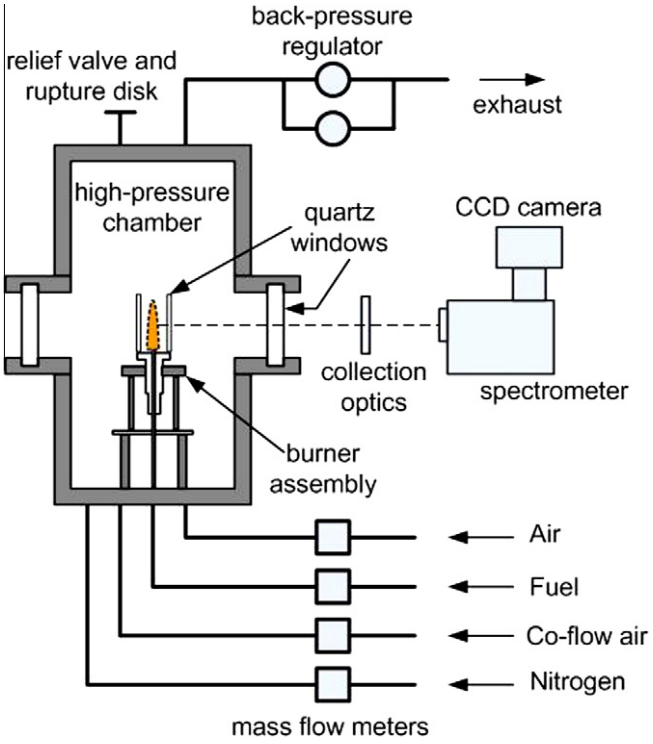

Fig. 1. A schematic of the experimental set-up.

2. Experimental

The experimental high-pressure combustion chamber and the laminar diffusion flame burner used in this study are described in detail in [7–10]. A schematic of the experimental set-up is shown in Fig. 1. The design pressure of the chamber is about 110 atm, and its internal diameter and internal height are 0.24 m and 0.6 m, respectively. Optical access into the chamber is through three ports at 0°, 90°, and 180° locations allowing line-of-sight measurements as well as 90° scattering and imaging experiments. A cut-off view of the chamber is shown in Fig. 2a. The burner has a fuel nozzle exit diameter of 3.06 mm and an air nozzle diameter of 25 mm, Fig. 2b. Sintered metal foam elements inserted into the fuel and air nozzles minimize the instabilities in the flow and create a top hat exit velocity profile.

The theory and overall experimental layout of the spectral soot emission diagnostic (SSE) are described previously [7,11]. In SSE, line-of-sight radiation emission from soot is measured along chords through the flame. A series of emission projections at a given height in the flame can be inverted to obtain radially resolved emission rates from which the temperature and the soot volume fraction can be determined when soot optical properties are known [12]. The emitted radiation from soot first passes through an adjustable aperture and lens unit. For the current study an aperture diameter of about 6.2 mm and an associated f-number of $f/48$ was used. The lens selected for this study is an achromatic doublet lens with a focal length of 300 mm. The lens has an anti-reflective coating, effective within the wavelength range of 650–1050 nm. The purpose of the lens is to image the flame radiation onto the entrance slit of the spectrometer. The lens is positioned to produce a 1:1 image. The entrance to the spectrometer contains two slits: the vertical slit is approximately 25 μm in width and the horizontal slit is approximately 290 μm in height. The slit sizes play a role in the resulting spatial resolution of the collected data.

The spectrometer is an imaging Czerny–Turner spectrometer that internally uses aspheric mirrors. The spectrometer grating

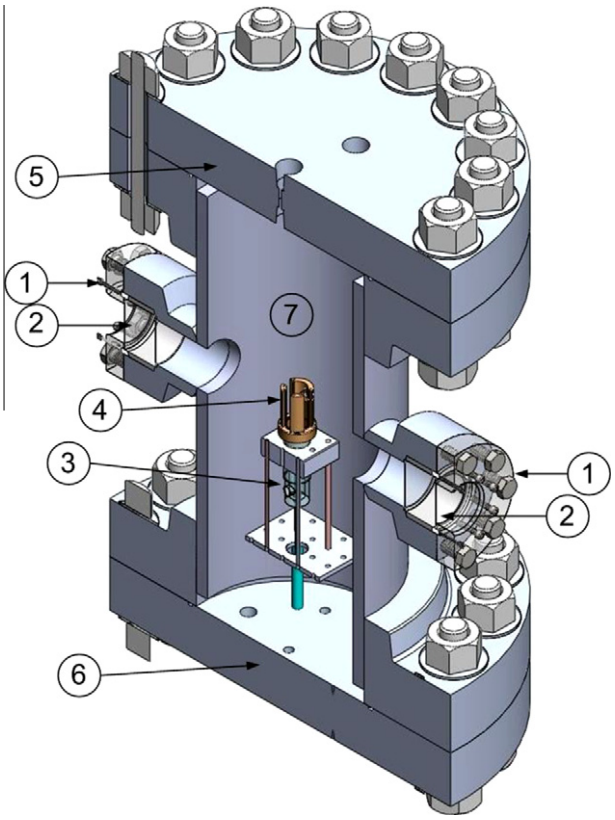

Fig. 2a. A cutaway view of the high-pressure chamber: 1 – optical access ports; 2 – quartz windows; 3 – burner assembly; 4 – Chimney assembly; 5 – upper flange housing the exhaust, safety valves, and pressure transducer; 6 – lower flange housing air, fuel pipes and wiring; 7 – combustion chamber.

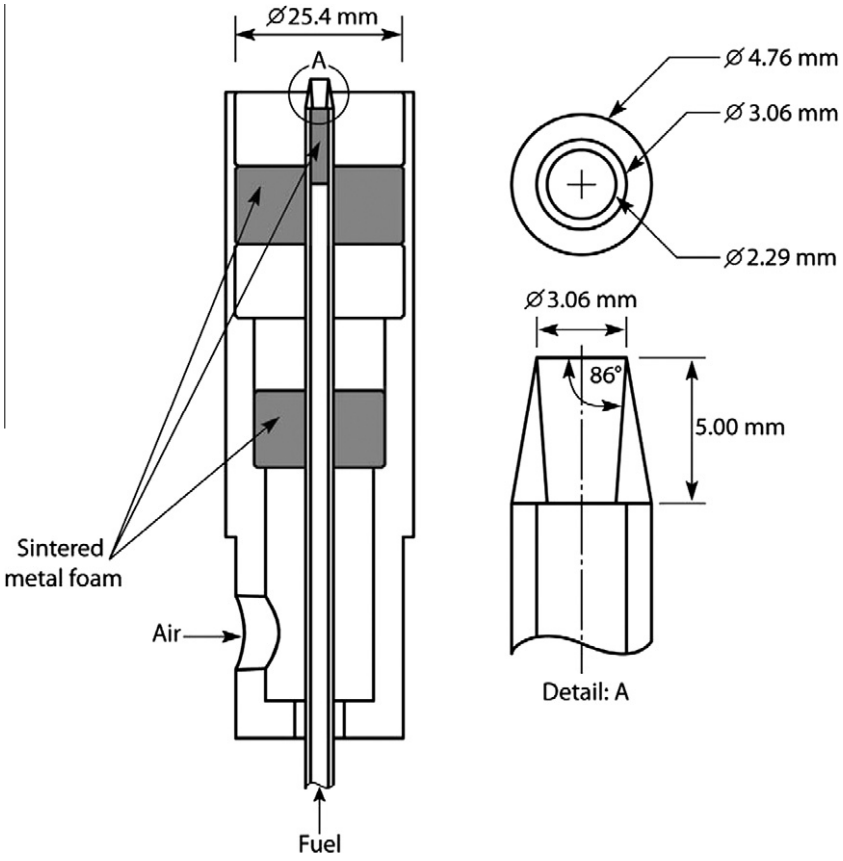

Fig. 2b. Details of the co-flow burner.

used for this task has a blaze wavelength of 775 nm and is manufactured with 300 groves/mm. The spectrometer has a dispersion of approximately 18.84 nm/mm. Soot emission is measured over a wavelength range of 690–945 nm.

The total array size of the CCD is 1340 × 400 pixels. However, due to the restricted size of the entrance slit, a region of interest of size 1340 × 80 pixels was selected. Combined with the previously mentioned spectrometer and grating, the CCD camera is capable of capturing an approximate wavelength spread of 505 nm across the camera array, providing a spectral step size of 0.377 nm/pixel. However the CCD resolution at FWHM (full width at half maximum) using 2.5 pixels, is approximately 0.942 nm. The horizontal spatial resolution was found to be approximately 70 μm. The vertical spatial resolution was inferred to be approximately 290 μm. To calibrate the spectral axis of the CCD array a pencil style neon calibration lamp was used. The system is calibrated for radiation intensity using a filament lamp, with a calibration traceable to NIST, placed inside the chamber. The uncertainty in the spectral radiance temperature is about 5 K. Further details of the experimental set-up and data reduction are given in [7–10].

In our previous soot studies at high pressures [7–10], the carbon mass flow rate for several fuels was kept constant at 0.41 mg/s. In the current study, we set the carbon mass flow rate with methane flames to 0.32 mg/s and 0.62 mg/s for the pressure ranges of 1–60 atm, and 1–20 atm, respectively. The carbon mass flow rate with ethane flames was 0.62 mg/s and the pressure range covered 1–15 atm. The fuel and carbon mass flow rates and the pressure ranges covered are summarized in Table 1 for previous measurements as well as for the current work. The upper pressure values were forced by either the fact that the flame was no longer a non-smoking flame (i.e., the fuel flow rate at that pressure reached the smoke point of the fuel) or the flame became highly flickering or unstable. For each pressure, measurements were obtained at height increments of 0.5 mm from the burner tip to the tip of the flame and at horizontal increments of 50 μm.

Table 1
Fuel and carbon mass flow rates and the pressure ranges of the previous measurements and the current data.

Fuel	Fuel flow rate (mg/s)	Fuel carbon rate (mg/s)	Pressure range (atm)	Source
Methane	0.55	0.41	10–60	[8]
	0.83	0.62	5–20	This work
	0.43	0.32	15–60	This work
Ethane	0.52	0.41	2–33	[10]
	0.78	0.62	2–15	This work
Propane	0.49	0.41	1–7.2	[9]

To assess the sensitivity of sooting propensity of the flame to pressure, previous studies suggested [4,7–10] that the percentage of total carbon in the fuel converted to soot, that is the soot yield, as a function of height is a better measure than the maximum line-of-sight integrated soot concentrations. The mass flow rate of carbon, in the form of soot, can be determined through the relationship

$$\dot{m}_s(z) = v_z(z)\rho_s \int 2\pi r f_v(r,z)dr \qquad (1)$$

where v_z is the axial velocity, ρ_s = 1.8 g/cm^3 is the soot density, and z is the axial height. The axial velocity is estimated using the relationship $v_z(z) = \sqrt{2az}$, where a is an acceleration constant commonly assumed to be 25 m/s^2 [4]. The soot yield, that is the percentage of carbon in the fuel converted to soot, is simply $Y_s = \dot{m}_s/\dot{m}_c$, where $\dot{m}_c$ is the carbon mass flow rate at the nozzle exit. The constant

acceleration assumption was used in our previous studies [7–10]; for the new sets of data reported in this work we used the same assumption for consistency and comparison. However, as will be explained in Section 3.2, this assumption has been relaxed and all soot yield data re-evaluated using numerically obtained flame velocity field.

3. Soot yields and scaling

3.1. Soot yields

The flame shape was found to change both in height, width and curvature with increasing pressure. However visible flame heights, as indicated by soot radiation, remained constant at pressures above 10 atm. For pressures lower than 1.0 MPa, visible flame heights tended to decrease and the blue flame region near the nozzle exit became more expansive as the pressure approached atmospheric pressure. Soot formation seemed to occur mainly at the tip of the flame for lower pressures, however as the pressure increased, the luminous carbon zone moved downward filling an increasingly larger portion of the flame as also noted in the previous high pressure experiments [7–10].

As the pressure was increased, axial flame diameters decreased giving an overall stretched appearance to the flame as noted previously [4,7–10]. The flame radius varied as, $r_f \propto P^{-0.5}$ and the flame cross-sectional area varied as, $A_f \propto P^{-1}$. This observation is in agreement with previous experimental results using methane, ethane and propane flames [8–10]. An inverse dependence on pressure for the flame cross-sectional area implies that residence times are independent of pressure which allows measurements to be compared at the same height above the burner exit.

Measured temperature and soot volume fraction distributions and their variation with pressure were very similar to previous measurements with methane and ethane at different fuel flow rates. Soot volume fraction profiles measured by SSE in ethane diffusion flames with a fuel flow rate of 0.78 mg/s are shown at various heights above the burner at 2, 5, 10, and 15 atm in Figs. 3–6. Measurements were made by scanning the entire flame diameter at each measurement height. However, the data shown in Figs. 3–6 represent averages of the left and right side scans. The soot forms first in an annular band near the burner rim, much like the atmospheric laminar diffusion flames. Near the mid height of the flame, the annular distribution of soot remains pronounced, but soot also begins to appear in the core of the flame. At the tip of the flame, the annular distribution disappears and a peak soot concentration is observed on the flame centerline (Fig. 7). Soot concentrations showed a significant increase with pressure; the peak soot volume fraction increased from about a few ppm at 2 atm to over 180 ppm at 15 atm (Fig. 6).

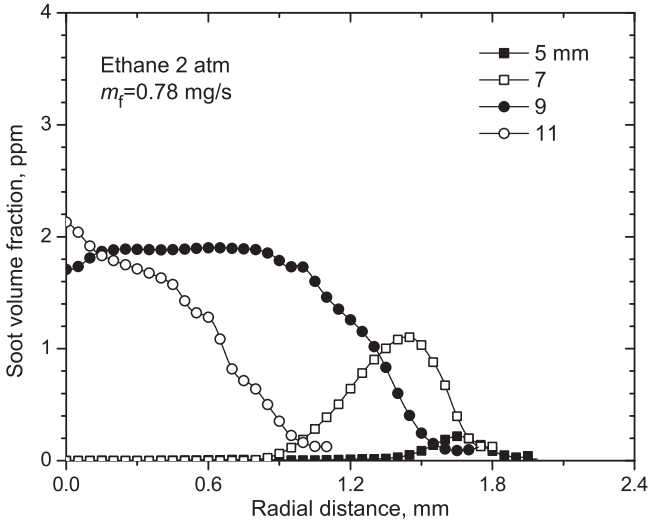

Fig. 3. Radial soot volume fraction profiles at 2 atm at various heights above the burner. Ethane–air flame at a fuel flow rate of 0.78 mg/s.

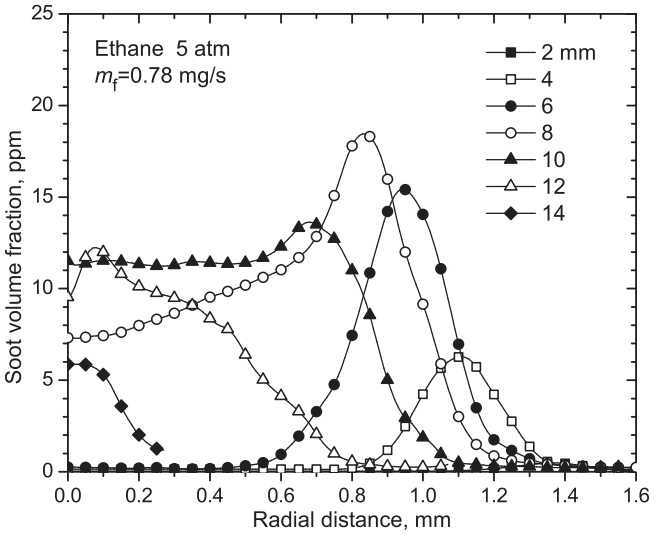

Fig. 4. Radial soot volume fraction profiles at 5 atm at various heights above the burner. Ethane–air flame at a fuel flow rate of 0.78 mg/s.

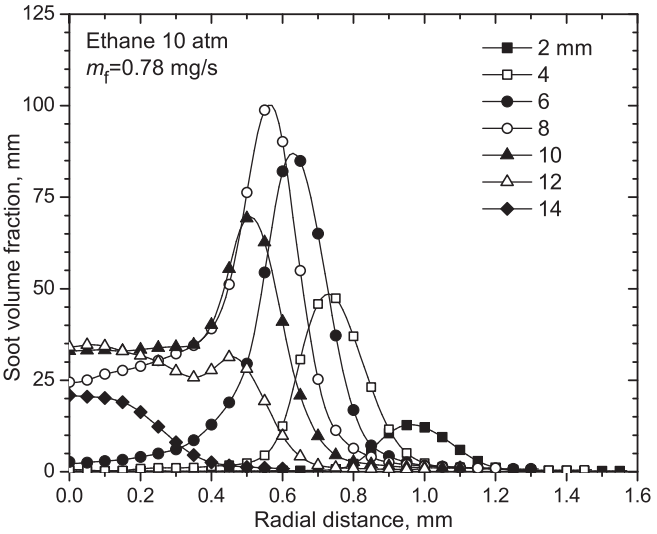

Fig. 5. Radial soot volume fraction profiles at 10 atm at various heights above the burner. Ethane–air flame at a fuel flow rate of 0.78 mg/s.

Averaged temperatures from the line-of-sight emission measurements through the flame centerline as a function of height along the flame axis at various pressures are shown in Fig. 7. It can be argued that the temperatures plotted in Fig. 7 represent a soot concentration-weighted average temperature along a chord through the flame centerline (perpendicular to the flame axis). Therefore, these temperatures should correspond closely to the peak soot volume fraction location temperatures [11].

Soot yields, calculated using Eq. (1), as a function of flame heights and pressure for methane flames are shown in Figs. 8 and 9, and for ethane flames in Fig. 10. For clarity, the soot yield data at 60 atm, which were very close to those at 50 atm, were not plotted in Fig. 8. It is noticeable that the soot yield data for

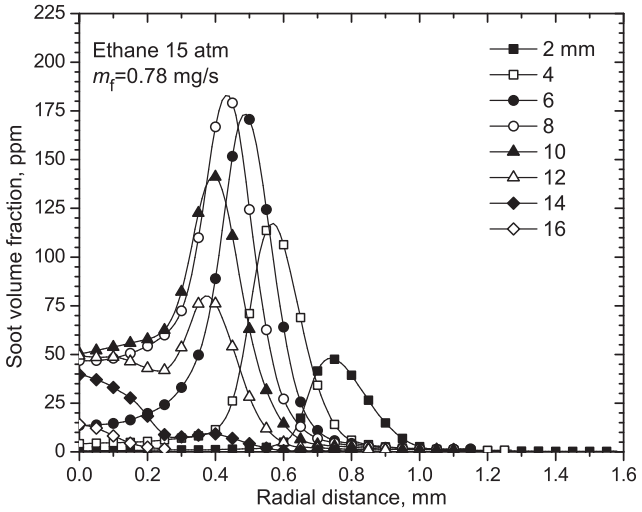

Fig. 6. Radial soot volume fraction profiles at 15 atm at various heights above the burner. Ethane–air flame at a fuel flow rate of 0.78 mg/s.

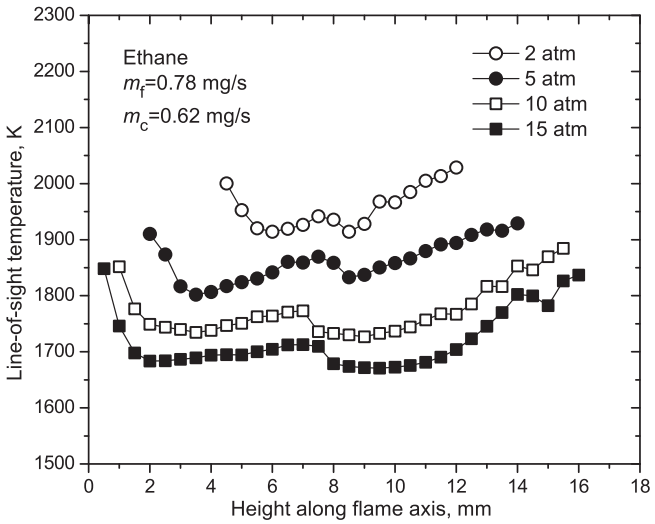

Fig. 7. Line-of-sight emission averaged soot temperature along the flame axis as a function of flame axial locations at various pressures. Ethane–air flame at a fuel flow rate of 0.78 mg/s.

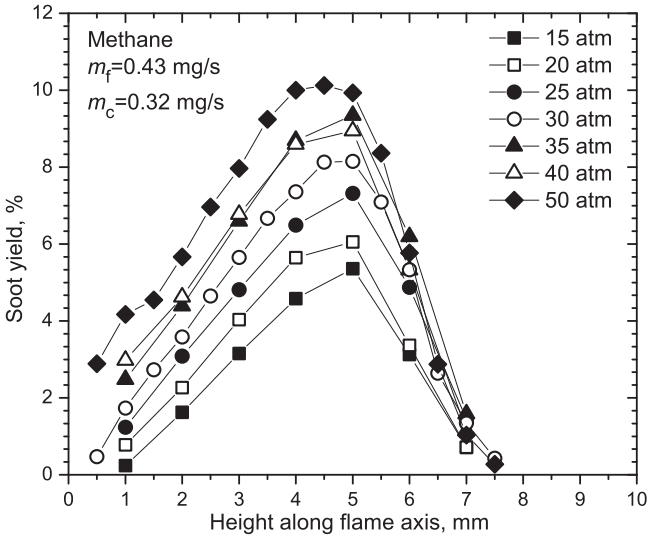

Fig. 8. Soot yields as a function of flame height at different pressures. Methane–air flame at a fuel flow rate of 0.43 mg/s. Note that, for clarity, data for 60 atm were not plotted: the soot yield values were almost identical with soot yields at 50 atm.

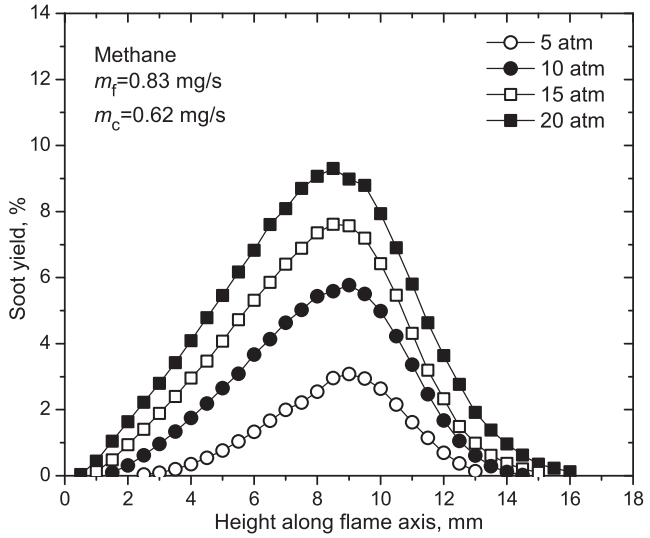

Fig. 9. Soot yields as a function of flame height at different pressures. Methane–air flame at a fuel flow rate of 0.83 mg/s.

the lower flow rate of methane flame is relatively noisy (Fig. 8) as compared to the higher flow rate soot yields (Figs. 9 and 10). Some of the potential reasons for this might be tied to the relatively smaller size of the flames in Fig. 8. Small size flame thermal structure seems to be influenced more by the preheating provided by the fuel nozzle [13], which is heated by the radiation from the flame. Furthermore, in calculating the soot yields from Eq. (1), axial velocity within the flame envelope is assumed to be uniform. As mentioned above, this assumption is not entirely justified especially at lower portions of the flame near to the nozzle exit with smaller height flames.

Soot yield profiles are similar in behaviour to the profiles obtained previously with different fuel flow rates. The maximum soot yields from Figs. 8–10 are plotted in Fig. 11 along with data from previous experiments as a function of pressure. The strong influence of pressure on maximum soot yield, as well as the influence of fuel type, is obvious in this plot. It seems that the initial response of the maximum soot yield to pressure is stronger with ethane and propane at lower pressures as compared to methane at similar fuel flow rates. As expected, as the fuel flow rate increases so does the maximum soot yield for a given fuel.

3.2. Scaled soot yields

It is shown that, to a first approximation, the height of a buoyancy-dominated laminar co-flow diffusion flame, established on a circular fuel nozzle, scales with molecular diffusivity, D, fuel flow rate, Q, mean flame temperature, T_f, and molar stoichiometric oxidizer to fuel ratio, S, as [14],

$$H \propto \frac{Q/T_f^{0.67}}{D\ln(1+1/S)} \propto \frac{1}{PT_f^{0.67}}\frac{\upsilon A}{D\ln(1+1/S)}, \qquad (2)$$

for a fixed mass flow rate of fuel. This relationship holds as long as the flame is at or under its smoke point. Here, υ is the mean fuel exit velocity, and A is the fuel nozzle exit area. This dependency that the flame height is proportional to the mass flow rate of the fuel also

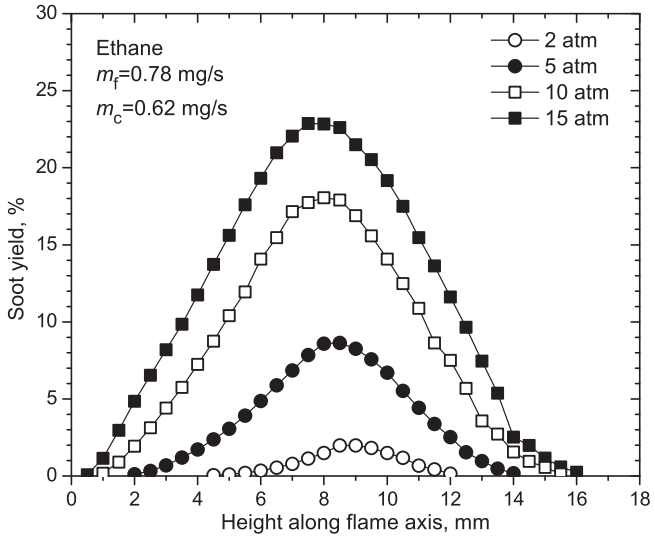

Fig. 10. Soot yields as a function of flame height at different pressures. Ethane–air flame at a fuel flow rate of 0.78 mg/s.

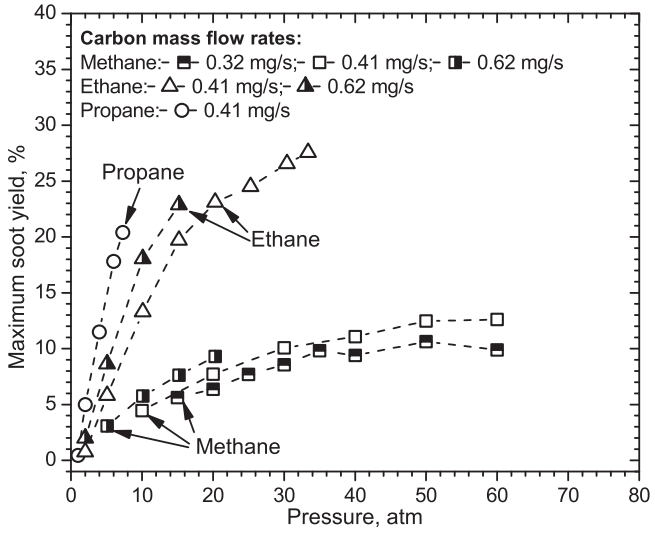

Fig. 11. Maximum soot yields of methane, ethane, and propane diffusion flames as a function of pressure at different fuel carbon flow rates.

holds at elevated pressures [8,10], that is the flame height stays constant as the pressure increases at a given fuel mass flow rate. Since the molecular diffusivity, D, is inversely proportional to pressure, P, i.e., $D \propto 1/P$, then the height of the diffusion flame is independent of the pressure. At a given height above the burner nozzle exit, the average velocity within the flame envelope will not change with pressure, if the flame cross-sectional area varies inversely with pressure. In other words, as the pressure increases, the material flow within the flame envelope will be through a narrower cross-section but at a higher density, thus keeping the average velocity constant at a given height [7,8]. This implies that the buoyant acceleration estimated by Roper et al. [15] for atmospheric flames is also valid for high pressure hydrocarbon–air flames to a first approximation. This argument assumes that the air entrainment into the flame envelope does not change much with pressure. As a result, the residence times in these flames scale with the square root of the flame height or square root of the fuel mass flow rate, that is $\tau \propto \sqrt{\dot{m}}$, where $\dot{m}$ is the fuel mass flow rate. For flames burning at conditions below their smoke point heights, soot yield will scale with the residence time, or $Y_s \propto \tau \propto \sqrt{\dot{m}}$.

It is argued in [16,17] that the maximum soot volume fraction scales with the enthalpy of combustion of the fuel. For most hydrocarbon fuels, the heat of combustion follows the stoichiometric air to fuel ratio closely, and the ratio of stoichiometric molar air to fuel ratio divided by the molecular mass of the fuel does not vary much at least for paraffinic fuels. On the other hand, at least for lower carbon number aliphatic fuels, soot yields seem to correlate with the molecular mass of the fuel [18,19], that is $Y_s \propto M$, where M is the molecular mass of the fuel.

In [17], it is shown that the peak soot formation rate in diffusion flames scales with the inverse of the hydrogen to carbon ratio of the hydrocarbon fuel. Assuming that this also holds at the elevated pressures, the soot yield will scale as $Y_s \propto 1/\varphi$, where φ is the hydrogen to carbon atomic ratio of the fuel. With the three scaling arguments given above, we have

$$Y_s \propto \frac{M\sqrt{\dot{m}}}{\varphi} \tag{3}$$

If the data plotted in Fig. 11 are reduced using Eq. (3), all points collapse to almost a single curve as shown in Fig. 12 when they are plotted versus the reduced pressure (pressure divided by the critical pressure of the fuel). In reducing the data in Fig. 11, the methane carbon mass flow rate $\dot{m}_r$ of 0.41 mg/s was taken as the reference, and the reduced maximum soot yields were calculated from

$$\psi = Y_s \frac{\varphi/\varphi_r}{(M/M_r)\sqrt{(\dot{m}/\dot{m}_r)}} \tag{4}$$

where the subscript r designates the properties of methane. In recent numerical studies, with diluted ethylene [20] and methane flames [21] at elevated pressures, it was found that the acceleration constant a, which is used to estimate the axial velocity of the flame as a function of height, is larger than 25 m/s^2. Instead of calculating the soot yield from Eq. (1) using the constant acceleration, the velocity field within the flame envelope computed from full simulation was used [20,21]. With this approach the maximum soot yields were systematically higher, about (28 ∓ 4)%, than the yields calculated with the constant acceleration assumption for methane flames. To take this into account, the data in Fig. 11 were adjusted by multiplying the soot yields by 1.28.

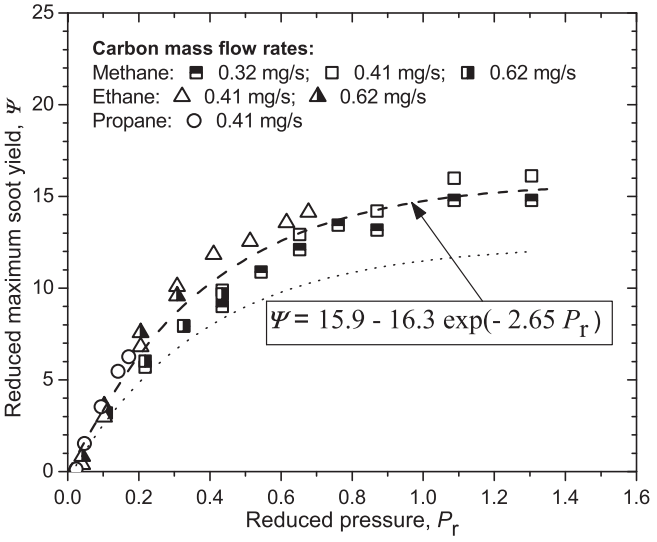

Fig. 12. Variation of the scaled maximum soot yields with reduced pressure. Dashed line is a least-square curve fit to the data.

4. Discussion

The behaviour of the reduced maximum soot yields in Fig. 12 seems to indicate that the soot yield reaches a plateau asymptotically as the pressure increases. The implications of this behaviour is that the pressure dependence of soot yield shows a power law relationship only at lower pressures; as pressure increases, the dependence of soot yield on pressure gradually decreases. This trend of the pressure dependence of the soot yield could be represented by an exponential expression. A least-square curve fit, in which the reduced pressure P_r is the independent variable, yields

$$\psi = a_o + a_1 \exp[-a_2 P_r] \quad (5)$$

where $a_o = 15.9$, $a_1 = -16.3$, and $a_2 = 2.65$ (Fig. 12). The dotted curve in Fig. 12 indicates the exponential fit to soot yield data evaluated using the constant acceleration of 25 m/s^2.

The rationale for using the reduced pressure as the correlating parameter is related to the dependence of the molecular diffusivity on the pressure. In laminar co-flow diffusion flames, as Eq. (2) indicates, the flame height, and hence the residence time, is inversely proportional to the molecular diffusivity. On the other hand, the molecular diffusivity scales with the inverse of pressure [22]. But the molecular diffusivity's dependence on the pressure starts deviating from the inverse relationship and the product of pressure and diffusivity is no longer constant but starts decreasing with increasing pressure when the reduced pressure P_r, ratio of actual pressure divided by the critical pressure of the gas, exceeds 0.5 [22], up to the critical point. At supercritical pressures, it seems that $D \propto P_r^{1/2}$ [22]. Since the molecular diffusivity shows a dependence on reduced pressure when $P_r \geqslant 0.5$, it seems logical to use the reduced pressure as the correlating parameter.

It should be noted that the above analysis implicitly assumes that the flame temperature differences among the three fuels are negligible. There is an expected increase in the flame temperature as the pressure is increased. However, in sooting flames, as the pressure increases so do the soot concentrations which in turn increases the heat loss by radiation from the flame. The end result is that the overall temperatures decrease slightly as the pressure is increased as shown in Fig. 7 as well as demonstrated in [7,10].

There are three important points regarding the information displayed in Fig. 12: (a) the maximum soot yield of gaseous fuels display a unified dependence on pressure, at least in paraffinic gaseous hydrocarbon fuel diffusion flames; (b) the maximum soot yield seems to reach a plateau asymptotically as the pressure exceeds the critical pressure of the fuel; and (c) when combined with the characteristic time scales and temperature histories, this type of unified soot yield behaviour may constitute the basis of relatively simple soot models for turbulent combustion codes. What is unknown currently is whether the liquid fuels, more precisely pure liquid paraffinic hydrocarbons, display a similar unified behaviour.

It should be emphasized that the simple scaling arguments are not claimed to be universal and may be valid only for hydrocarbons within a specific homologous series, such as *n*-paraffins. Normalization of soot yields among homologous series might require additional scaling, such as smoke point (or some other measure of sooting propensity). Furthermore, the scaling proposed by Eq. (5) is only valid for the axysymmetric and buoyancy-dominated laminar diffusion flames.

Some degree of uncertainty is introduced to the measured temperature and soot volume fractions due to a lack of understanding of the dependence of soot optical properties, specifically soot refractive index and consequently the refractive index absorbtion function $E(m)$, on soot temperature, and wavelength. The results of a limited number of studies on the dependence of refractive index on soot temperature reveal that at typical flame temperatures the dependence is not significant. We assumed, for the purposes of this work and to be consistent with the previous high-pressure soot measurements [7–10], that soot refractive index does not have a significant dependence on temperature.

Another source of uncertainty originates from the dependence of the function $E(m)$, which is a function of soot refractive index, on wavelength. Based on the previous analysis and estimates [11,23] a constant $E(m)$ function with a magnitude of 0.274 is assumed in the present work. This is consistent with the results of Krishnan et al. [23] and the previous measurements with methane [7,8] and propane flames [9].

Modelling of the flame emission using the previously described methods [11] showed that attenuation of emission by soot introduces only a small error in the measurements (i.e., <2%) for even the highest soot loadings observed in these flames. This result may seem surprising considering that soot yields exceeding 25% have been measured in ethane flame. However, light attenuation is a function of the product of the soot concentration and the absorption path length. Although soot concentrations are a factor of ten larger than those observed in the familiar atmospheric flames, e.g. [24,25], the flame diameter is much smaller and decreases with increasing pressure. A more detailed discussion of the subject can be found in [26].

Reliable measurements using the SSE method were only possible in radial regions around the emission intensity annulus as noted previously [7–10]. The total uncertainty of the temperature and soot volume fraction measurements is dominated by the systematic uncertainty of the soot refractive index as discussed above. The uncertainty in soot yield due to random errors was estimated as 30% at 2 atm, and less than 8% at higher pressures [27–29]. The total uncertainty in temperature measurements was evaluated as 3.5% [27–29].

5. Concluding remarks

The soot yields (defined as the mass flow of soot at a given flame height cross-section per mass flow of carbon in the fuel) in co-flow methane–air and ethane–air laminar diffusion flames at elevated pressures were measured at different fuel flow rates than reported previously. Available high-pressure soot yield data along with the data obtained in the current study from gaseous fuel diffusion flames were shown to display a unified dependence on reduced pressure when the soot yield is properly scaled. The maximum soot yield seems to reach a plateau asymptotically as the pressure exceeds the critical pressure of the fuel. Although the observed unified behaviour is for methane, ethane, and propane diffusion flames only, it has the potential to constitute the basis of relatively simple soot models when combined with the characteristic time scales and temperature histories.

Acknowledgments

Operational funds for this work have been provided by Natural Sciences and Engineering Research Council (NSERC) and Canadian Space Agency (CSA).

References

[1] C.H. Kim, F. Xu, G.M. Faeth, Combust. Flame 152 (2008) 301–316.
[2] F. Liu, K. Thomson, H. Guo, G.J. Smallwood, Combust. Flame 146 (2006) 456–471.
[3] I.M. Miller, H.G. Maahs, High-Pressure Flame Systems for Pollution Studies with Results for Methane–Air Diffusion Flames, TN D-8407, NASA, 1977.
[4] W.L. Flower, C.T. Bowman, Proc. Combust. Inst. 21 (1988) 1115–1124.
[5] W. Lee, Y.D. Na, J. Soc, Mech. Eng. Int. J. Ser. B 43 (2000) 550–555.
[6] L.L. McCrain, W.L. Roberts, Combust. Flame 140 (2005) 60–69.

[7] K.A. Thomson, Ö.L. Gülder, E.J. Weckman, R.A. Fraser, G.J. Smallwood, D.R. Snelling, Combust. Flame 140 (2005) 222–232.
[8] H.I. Joo, Ö.L. Gülder, Proc. Combust. Inst. 32 (2009) 769–775.
[9] D.S. Bento, K.A. Thomson, Ö.L. Gülder, Combust. Flame 145 (2006) 765–778.
[10] P.M. Mandatori, Ö.L. Gülder, Proc. Combust. Inst. 33 (2011) 577–584.
[11] D.R. Snelling, K.A. Thomson, G.J. Smallwood, Ö.L. Gülder, E.J. Weckman, R.A. Fraser, AIAA J. 40 (9) (2002) 1789–1795.
[12] C.J. Dasch, Appl. Opt. 31 (8) (1992) 1146–1152.
[13] Ö.L. Gülder, K.A. Thomson, D.R. Snelling, Combust. Flame 144 (2006) 426–433.
[14] F.G. Roper, Combust. Flame 29 (1977) 219–226.
[15] F.G. Roper, C. Smith, A.C. Cunningham, Combust. Flame 29 (1977) 227–234.
[16] J.H. Kent, Combust. Flame 63 (1986) 349–358.
[17] Ö.L. Gülder, Combust. Flame 78 (1989) 179–194.
[18] H.F. Calcote, D.M. Manos, Combust. Flame 49 (1983) 289–304.
[19] D.B. Olson, J.C. Pickens, R.J. Gill, Combust. Flame 62 (1985) 43–60.
[20] M.R.J. Charest, I.H. Joo, Ö.L. Gülder, C.P.T. Groth, Proc. Combust. Inst. 33 (2011) 549–557.
[21] M.R.J. Charest, Ö.L. Gülder, C.P.T. Groth, Combust. Flame 158 (2011) 860–875.
[22] R.C. Reid, J.M. Prausnitz, B.E. Poling, The Properties of Gases and Liquids, fourth ed., McGraw Hill, 1987 (Chapter 11).
[23] S.S. Krishnan, K.-C. Lin, G.M. Faeth, J. Heat Transfer 122 (2000) 517–524.
[24] D.R. Snelling, K.A. Thomson, G.J. Smallwood, Ö.L. Gülder, Appl. Opt. 38 (12) (1999) 2478–2485.
[25] R.J. Santoro, T.T. Yeh, J.J. Horvath, H.G. Semerjian, Combust. Sci. Technol. 53 (2–3) (1987) 89–115.
[26] J.J. Murphy, C.R. Shaddix, Combust. Flame 143 (2005) 1–10.
[27] K.A. Thomson, PhD Thesis, University of Waterloo, Waterloo, Canada, 2005.
[28] D.S. Bento, MASc Thesis, UTIAS University of Toronto, Toronto, Canada, 2005.
[29] P.M. Mandatori, MASc Thesis, UTIAS University of Toronto, Toronto, Canada, 2006.